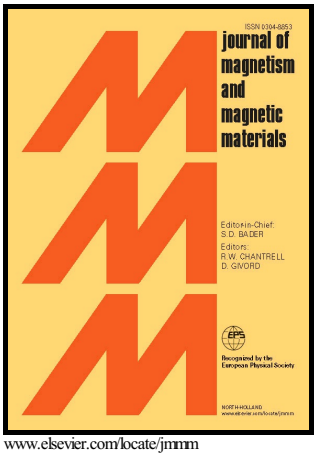

www.elsevier.com/locate/jmmm

Ground states, magnetization plateaus and bipartite entanglement of frustrated spin-1/2 Ising-Heisenberg and Heisenberg triangular tubes

Raphael C. Alécio, Marcelo L. Lyra, Jozef Strečka

PII: S0304-8853(16)30807-1
DOI: http://dx.doi.org/10.1016/j.jmmm.2016.05.081
Reference: MAGMA61495

To appear in: *Journal of Magnetism and Magnetic Materials*

Received date: 14 March 2016
Revised date: 2 May 2016
Accepted date: 24 May 2016

Cite this article as: Raphael C. Alécio, Marcelo L. Lyra and Jozef Strečka Ground states, magnetization plateaus and bipartite entanglement of frustrate spin-1/2 Ising-Heisenberg and Heisenberg triangular tubes, *Journal of Magnetisn and Magnetic Materials,* http://dx.doi.org/10.1016/j.jmmm.2016.05.081

Ground states, magnetization plateaus and bipartite entanglement of frustrated spin-1/2 Ising-Heisenberg and Heisenberg triangular tubes

Raphael C. Alécio, Marcelo L. Lyra

Instituto de Física, Universidade Federal de Alagoas, 57072-970, Maceió-AL, Brazil

Jozef Strečka

Department of Theoretical Physics and Astrophysics, Faculty of Science, P. J. Šafárik University, Park Angelinum 9, 040 01 Košice, Slovakia

Abstract

The ground-state phase diagram, magnetization process and bipartite entanglement of the frustrated spin-1/2 Ising-Heisenberg and Heisenberg triangular tube (three-leg ladder) are investigated in a non-zero external magnetic field. The exact ground-state phase diagram of the spin-1/2 Ising-Heisenberg tube with Heisenberg intra-rung and Ising inter-rung couplings consists of six distinct gapped phases, which manifest themselves in a magnetization curve as intermediate plateaus at zero, one-third and two-thirds of the saturation magnetization. Four out of six available ground states exhibit quantum entanglement between two spins from the same triangular unit evidenced by a non-zero concurrence. Density-matrix renormalization group calculations are used in order to construct the ground-state phase diagram of the analogous but purely quantum spin-1/2 Heisenberg tube with Heisenberg intra- and inter-rung couplings, which consists of four gapped and three gapless phases. The Heisenberg tube shows a continuous change of the magnetization instead of a plateau at zero magnetization, while the intermediate one-third and two-thirds plateaus may be present or not in the zero-temperature magnetization curve.

Keywords: spin tube; geometric frustration; magnetization plateau; quantum entanglement

1. Introduction

Geometrically frustrated quantum spin models represent fascinating topics of current research interest emerging at the border of condensed matter physics [1] and quantum information [2, 3]. Recent interest in quantum spin models from the perspective of quantum information and computation has been stimulated mainly by the fact that these models provide indispensable ground for the development and further testing of entanglement measures within realistic models of real many-body solid-state systems [2, 3]. A quantum spin model is said to be geometrically frustrated when the spins cannot simultaneously satisfy all underlying pair interactions [4]. For example, any lattice built up from elementary triangular plaquettes will be subject to a geometric spin frustration provided that antiferromagnetic interactions are assumed [1, 5].

One-dimensional (1D) quantum spin systems deserve a special mention among the wide class of geometrically frustrated models, because they are basically affected by the mutual interplay between the geometric spin frustration and extraordinarily strong quantum fluctuations. Geometrically frustrated 1D quantum spin models display exotic quantum ground states such as the gapped dimerized [6, 7] and Haldane-like phases [8, 9] with a peculiar topological order, or the gapless one- or two-component Tomonaga-Luttinger spin-liquid phases [10]. Another intriguing feature of geometrically frustrated 1D quantum spin systems lies in the presence of spin gap [11] and quantized plateaus in the magnetization pro-

cess [12, 13, 14]. The existence of fractional plateaus in the zero-temperature magnetization curve of 1D quantum spin systems is restricted by the quantization condition $p(S_u - m_u) \in Z$ (p is the period of the ground state, S_u and m_u are the total spin and total magnetization of the unit cell), which is known as the Oshikawa-Yamanaka-Affleck rule [15, 16]. According to this rule, the number of available plateaus can be lifted either by increasing the total spin of the unit cell S_u or by breaking the translational symmetry (i.e. by increasing p).

Bearing this in mind, the spin-1/2 triangular tube with antiferromagnetic interactions represents a valuable example of a 1D frustrated spin model, which has large enough total spin per unit cell ($S_u = 3/2$) and is simultaneously accessible to a spontaneous symmetry breaking. The magnetization plateaus at zero, one-third and two-thirds of the saturation moment can accordingly occur in the zero-temperature magnetization curve of the spin-1/2 triangular tube once the period of the ground state is doubled ($p = 2$). Whether or not those magnetization plateaus indeed emerge may basically depend on the competition between the intra-triangle and inter-triangle coupling constants [17]. For instance, the experimental realization of the frustrated spin-1/2 Heisenberg triangular tube $[(CuCl_2tachH)_3Cl]Cl_2$ (tach=1,3,5-triaminocyclohexane) does not show any magnetization plateau, since the inter-triangle coupling constant is much stronger than the intra-triangle interaction [18, 19].

Another interesting aspect of the spin-1/2 Heisenberg triangular tube concerns with the spin chirality. It has been demonstrated that the geometric spin frustration may cause a spin chirality order in the presence of a small magnetic field or a small exchange anisotropy [20, 21, 22]. Quite recently, we have proposed and exactly solved a simplified version of the spin-1/2 Ising-Heisenberg triangular tube with the Heisenberg intra-rung and the Ising inter-rung coupling in the absence of an external magnetic field [23]. In spite of a certain over-simplification, the frustrated spin-1/2 Ising-Heisenberg tube also shows one peculiar ground state with a high macroscopic degeneracy due to the chiral degrees of freedom of elementary triangular plaquettes. In addition, one generally detects an anomalous behavior of basic thermodynamic quantities (entropy, specific heat) when the spin-1/2 Ising-Heisenberg tube is driven sufficiently close to a phase boundary with the macroscopically degenerate ground state, which is quite reminiscent of a thermally-induced first-order phase transition [23].

In the present work, we will focus our attention to the ground-state properties of two frustrated spin-1/2 Ising-Heisenberg and Heisenberg triangular tubes. The former spin-1/2 Ising-Heisenberg tube with the Ising inter-rung coupling is fully exactly tractable, because it can be effectively mapped to a classical composite spin-chain model by making use of the total spin of the elementary triangular unit. By contrast, the latter spin-1/2 Heisenberg tube with the Heisenberg inter-rung coupling can be mapped following the same procedure to a quantum composite spin-chain model, which can be subsequently treated by density-matrix renormalization group (DMRG) calculations. For both considered models we will report the ground-state phase diagrams, magnetization curves and the pair correlation functions, which will be subsequently used to quantify the bipartite quantum entanglement within the relevant ground states.

The organization of this paper is as follows. The frustrated spin-1/2 Ising-Heisenberg tube is introduced in Sec. 2 along with its exact analytical treatment. Sec. 3 briefly describes the details of DMRG calculations for the analogous but purely quantum spin-1/2 Heisenberg tube. The most interesting results for the ground state, magnetization process, pair correlation functions and bipartite entanglement are presented in Sec. 4. Finally, a few concluding remarks are drawn in Sec. 5.

2. Ising-Heisenberg tube

Let us consider the frustrated spin-1/2 Ising-Heisenberg triangular tube (three-leg ladder) schematically illustrated in Fig. 1, which takes into account the Heisenberg intra-rung interaction, the Ising inter-rung interaction and the effect of external magnetic field. The XXZ Heisenberg intra-rung coupling is assigned to all spin pairs belonging to the same triangular rung, while the Ising inter-rung interaction is supposed between all spin pairs from nearest-neighbor triangular rungs. It is worth noticing that the triangular tube can be alternatively viewed as the frustrated three-leg ladder with periodic boundary condition along the rung direction, from which the terminology of both considered coupling constants follows. The spin-1/2 Ising-Heisenberg tube is defined

by the following Hamiltonian

$$\hat{H} = \sum_{i=1}^{N}\sum_{j=1}^{3}\left[J_x\left(\hat{S}^x_{i,j}\hat{S}^x_{i,j+1}+\hat{S}^y_{i,j}\hat{S}^y_{i,j+1}\right)+J_z\hat{S}^z_{i,j}\hat{S}^z_{i,j+1}\right] + J_1\sum_{i=1}^{N}\left(\sum_{j=1}^{3}\hat{S}^z_{i,j}\right)\left(\sum_{j=1}^{3}\hat{S}^z_{i+1,j}\right)-h\sum_{i=1}^{N}\sum_{j=1}^{3}\hat{S}^z_{i,j}, \quad (1)$$

where $\hat{S}^{\alpha}_{i,j}$ stands for the standard spin-1/2 operator, the superscript $\alpha \in x,y,z$ denotes its respective spatial component, the subscript $j = 1,2,3$ labels the lattice position within the i-th triangular rung and periodic boundary conditions $S_{i,4} \equiv S_{i,1}$, $S_{N+1,j} \equiv S_{1,j}$ are imposed (see Fig. 1). The interaction terms J_x and J_z specify the spatially anisotropic XXZ Heisenberg intra-rung interaction between the spin pairs from the same triangular rung, the coupling constant J_1 labels the Ising inter-rung interaction between the spin pairs from the nearest-neighbor triangular rungs and the field term h takes into account the Zeeman's energy. The spin-1/2 Ising-Heisenberg triangular tube defined by the Hamiltonian (1) is a natural extension of the model introduced in our preceding work [23], which additionally takes into account the effect of external magnetic field.

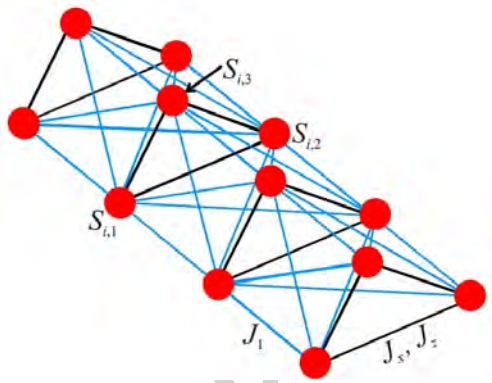

Figure 1: A diagrammatic representation of the frustrated spin-1/2 Ising-Heisenberg triangular tube. Thick (black) lines represent the XXZ Heisenberg intra-rung coupling (J_x, J_z), while thin (blue) lines correspond to the Ising inter-rung coupling (J_1).

The Hamiltonian (1) of the spin-1/2 Ising-Heisenberg tube can be alternatively rewritten in terms of the total spin of the Heisenberg spin triangles $\hat{\vec{T}}_i = \sum_{j=1}^{3}\hat{\vec{S}}_{i,j}$ and its z-component $\hat{T}^z_i = \sum_{j=1}^{3}\hat{S}^z_{i,j}$. Using the spin identity $(\hat{T}^{\alpha}_i)^2 = \frac{3}{4} - 2(\hat{S}^{\alpha}_{i,1}\hat{S}^{\alpha}_{i,2}+\hat{S}^{\alpha}_{i,2}\hat{S}^{\alpha}_{i,3}+\hat{S}^{\alpha}_{i,3}\hat{S}^{\alpha}_{i,1})$, the total Hamiltonian (1) can be recast into the form

$$\hat{H} = -\frac{3N}{8}(2J_x + J_z) + \sum_{i=1}^{N}\hat{H}_i, \quad (2)$$

where the first term is a less important constant and the second term is the sum of symmetrically defined Hamiltonians $\hat{H}_i$ each involving two consecutive composite spin operators $\hat{\vec{T}}^2_i$, $\hat{\vec{T}}^2_{i+1}$ and their z-components

$$\hat{H}_i = J_1\hat{T}^z_i\hat{T}^z_{i+1} + \frac{J_x}{4}(\hat{\vec{T}}^2_i + \hat{\vec{T}}^2_{i+1}) + \frac{J_z - J_x}{4}[(\hat{T}^z_i)^2 + (\hat{T}^z_{i+1})^2] - \frac{h}{2}(\hat{T}^z_i + \hat{T}^z_{i+1}). \quad (3)$$

Apparently, the total spin of the i-th Heisenberg spin triangle (rung) and its z-component are conserved quantities with well defined quantum numbers, because the corresponding spin operators commute with the total Hamiltonian (1). The eigenvalues of the Hamiltonian (3) can be accordingly expressed through the eigenvalues of the composite spin operators $\hat{\vec{T}}^2_i$ and $\hat{T}^z_i$. The basic quantum-mechanical law for the composition of spin angular momenta implies that the eigenvalues of the composite spin operators $\hat{\vec{T}}^2_i$ and $\hat{T}^z_i$ are quantized according to the rules $T_i(T_i+1)$ with $T_i = \{1/2, 3/2\}$ and $T^z_i = \{-T_i, -T_i+1, \ldots, T_i\}$, respectively. In this regard, the Hamiltonian (3) has been put into a fully diagonal form and its respective eigenvalues are given by

$$E_i = J_1T^z_iT^z_{i+1} + \frac{J_x}{4}[T_i(T_i+1) + T_{i+1}(T_{i+1}+1)] + \frac{J_z - J_x}{4}[(T^z_i)^2 + (T^z_{i+1})^2] - \frac{h}{2}(T^z_i + T^z_{i+1}). \quad (4)$$

By introducing the total spin for the Heisenberg spin triangles (rungs) one consequently obtains an exact mapping equivalence between the Hamiltonians of the spin-1/2 Ising-Heisenberg triangular tube and the classical composite spin-chain model, in which the Ising interaction J_1 determines the nearest-neighbor coupling between z-components of the composite spins, the XXZ Heisenberg interaction (J_x, J_z) shifts the energy corresponding to two possible values of the composite spins $T_i = 1/2$, $3/2$, and respectively, the external magnetic field h acts on z-component of the composite spins T^z_i. The complete set

of eigenstates of the spin-1/2 Ising-Heisenberg tube can be obtained from Eqs. (2) and (4) after taking into consideration all available combinations of the quantum spin numbers T_i and T_i^z for each i, from which all possible ground states can be easily constructed by extending the lowest-energy eigenstate (4) to the whole triangular spin tube (see the section 4).

It is quite clear that the expectation values for the nearest-neighbor pair correlation functions $C_{\alpha\alpha} = \langle \hat{S}^{\alpha}_{i,j} \hat{S}^{\alpha}_{i,j+1} \rangle$ and the averaged magnetization $m = \langle \hat{S}^{z}_{i,j} \rangle$ can be readily calculated once all available ground states of the spin-1/2 Ising-Heisenberg tube are found. These quantities gain an insight into the local spin arrangement inherent to the relevant ground states, but they can be alternatively explored for the computation of the degree of quantum entanglement within unusual quantum ground states. One of the most common measures of bipartite quantum entanglement is the so-called entanglement of formation (E_f) defined as [24]

$$\mathrm{E}_f(\rho) = min\{ \sum_i p_i \mathrm{S}(\rho_{A,i}) \}, \tag{5}$$

where the minimum is taken over all realizations of $\rho_{AB} = \sum_j p_j |\psi_j\rangle\langle\psi_j|$, and $\mathrm{S}(\rho_{A,i})$ is the von Neumann entropy of the reduced density matrix $\rho_{A,i} = \mathrm{Tr}_B |\psi_i\rangle\langle\psi_i|$. The expression for entanglement of formation E_f reduces in the special case of the quantum entanglement between two qubits to the following form

$$\mathrm{E}_f(\rho) = - \sum_{a=\pm 1} \frac{\sqrt{1+a\mathrm{C}}}{2} \ln \left(\frac{\sqrt{1+a\mathrm{C}}}{2} \right), \tag{6}$$

which monotonically depends on the concurrence [24]

$$\mathrm{C} = max\{0; 2\lambda_{max} - \mathrm{Tr}[R]\}. \tag{7}$$

Here, λ_{max} is the largest eigenvalue of the positive Hermitian matrix $R = \sqrt{\rho}(\sigma^y \otimes \sigma^y)\rho^*(\sigma^y \otimes \sigma^y)\sqrt{\rho}$, ρ^* is the complex conjugate of the reduced density matrix ρ and σ^y is the relevant Pauli matrix. Because the entanglement of formation (6) is a monotonous function of the concurrence (7), the latter quantity can be also used as a quantum entanglement estimator. The non-zero elements of the density matrix ρ for two spin-1/2 particles coupled through the XXZ Heisenberg interaction are given by [25]

$$\begin{aligned} \rho_{11} &= \frac{1}{4} + m + C_{zz}, \\ \rho_{22} &= \rho_{33} = \frac{1}{4} - C_{zz}, \\ \rho_{44} &= \frac{1}{4} - m + C_{zz}, \\ \rho_{23} &= \rho_{32} = 2C_{xx}, \end{aligned} \tag{8}$$

whereas all other matrix elements are null. The concurrence between two spin-1/2 particles interacting via the XXZ Heisenberg coupling then follows from the formula [25]

$$\mathrm{C} = max\{0; 4|C_{xx}| - 2\sqrt{\left(\frac{1}{4} + C_{zz}\right)^2 - m^2}\}. \tag{9}$$

As one can see, the two-qubit concurrence can be calculated from the expectation values of two spatial components of the pair correlation function and the magnetization, whereas it vanishes whenever there are no quantum correlations between two spins and becomes unity for maximally entangled spins [26].

3. Heisenberg tube

It might be quite interesting to contrast the exact results reported for the spin-1/2 Ising-Heisenberg triangular tube with the results for the analogous but fully quantum spin-1/2 Heisenberg triangular tube, which is defined through the Hamiltonian

$$\begin{aligned} \hat{H} &= J \sum_{i=1}^{N} \sum_{j=1}^{3} \hat{\vec{S}}_{i,j} \cdot \hat{\vec{S}}_{i,j+1} \\ &+ J_1 \sum_{i=1}^{N} \left(\sum_{j=1}^{3} \hat{\vec{S}}_{i,j} \right) \cdot \left(\sum_{j=1}^{3} \hat{\vec{S}}_{i+1,j} \right) \\ &- h \sum_{i=1}^{N} \sum_{j=1}^{3} \hat{S}^{z}_{i,j}. \end{aligned} \tag{10}$$

The interaction terms J and J_1 have similar meaning as described previously for the spin-1/2 Ising-Heisenberg tube with the exception that they both refer to the isotropic

Heisenberg couplings. The spin-1/2 Heisenberg triangular tube belongs to a class of frustrated ladders comprehensively studied in Ref. [17], so let us recall just a few crucial steps of its rigorous treatment. At first, the total Hamiltonian (10) of the spin-1/2 Heisenberg tube will be rewritten using the total spin of the i-th rung $\hat{\vec{T}}_i = \sum_{j=1}^{3} \hat{\vec{S}}_{i,j}$ and its z-component $\hat{T}_i^z = \sum_{j=1}^{3} \hat{S}_{i,j}^z$

$$\hat{H} = - \frac{3N}{4} J + \sum_{i=1}^{N} [J_1 \hat{\vec{T}}_i \cdot \hat{\vec{T}}_{i+1} + \frac{J}{4}(\hat{\vec{T}}_i^2 + \hat{\vec{T}}_{i+1}^2) - \frac{h}{2}(\hat{T}_i^z + \hat{T}_{i+1}^z)]. \quad (11)$$

It is quite evident that one obtains a similar composite spin-chain model as obtained previously for the spin-1/2 Ising-Heisenberg tube [cf. Eq. (11) with Eqs. (2) and (3) considering the particular case $J_x = J_z = J$], but the nearest-neighbor coupling J_1 between the composite spins is presently the isotropic Heisenberg coupling rather than the simpler Ising coupling. Hence, it follows that the composite spin-chain model defined through the Hamiltonian (11) is still not in a fully diagonal form and preserves a quantum character. However, the total spin of the i-th rung and its z-component remain conserved quantities with well defined quantum numbers, which allows one to get rid of a geometric spin frustration and to employ the state-of-the-art numerical calculations based on DMRG or QMC methods in order to obtain precise numerical results. In addition, it turns out that the total spin of rung is either the same or regularly alternates within all available ground states [17], which means that the ground states of the spin-1/2 Heisenberg tube can be obtained from the numerical simulation of only three composite spin-chain models:

- the effective spin-3/2 Heisenberg chain with the overall energy

$$E_{3/2} = \frac{3}{4} NJ + J_1 E^{3/2}(N, S_T^z), \quad (12)$$

- the effective mixed spin-(1/2,3/2) Heisenberg chain with the energy

$$E_{1/2-3/2} = J_1 E^{1/2-3/2}(N, S_T^z), \quad (13)$$

- the effective spin-1/2 Heisenberg chain with the corresponding energy

$$E_{1/2} = -\frac{3}{4} NJ + J_1 E^{1/2}(N, S_T^z). \quad (14)$$

In above, $E^{\star}(N, S_T^z)$ denotes the energy of the effective Heisenberg chain of N composite spins given by the Hamiltonian $\hat{H}_{eff} = \sum_{i=1}^{N} \hat{\vec{T}}_i \cdot \hat{\vec{T}}_{i+1}$ within the sector with the total spin $S_T^z = \sum_{i=1}^{N} T_i^z$ (the coupling constant is set to unity within the effective model). It is worthwhile to remark that each spin state $T_i = 1/2$ comes with two different chiralities. The eigenvalues of the Hamiltonian (10) are independent of these two chiralities, but this degeneracy gives rise to an entropy $k_B \ln 2$ per each rung with the total spin $T_i = 1/2$.

The ground-state phase diagram and magnetization process of the spin-1/2 Heisenberg triangular tube has been previously investigated using DMRG simulations [27] for the effective chains of 60 composite spins [17]. In the present work, we have adapted the open source software from Algorithms and Libraries for Physics Simulations (ALPS) project [28] in order to perform DMRG simulations for the larger effective chains of 120 composite spins, which correspond to the spin-1/2 Heisenberg triangular tube of 360 spins. The DMRG simulations have been performed with 16 sweeps at the target system size, whereas the number of kept states was raised up to 1000 during the final sweeps. The large number of sweeps was necessary because of the choice of periodic boundary conditions. We have found the following lowest energies for three composite spin-chain models: $E^{1/2}(120, 0) = -0.44320$, $E^{1/2-3/2}(120, 0) = -0.98361$ and $E^{3/2}(120, 0) = -2.82832$, which agree well with the numerical data reported previously. Consequently, it was possible to estimate the ground-state energy of an infinite chain with an accuracy of 10^{-4} using Eq. (10) - (14) without any extrapolation (except for special values of the field where the magnetization jumps).

4. Results and discussion

In this section, let us proceed to a discussion of the most interesting results for the frustrated spin-1/2 Ising-Heisenberg and Heisenberg triangular tubes in an applied external magnetic field by assuming the particular case

with the antiferromagnetic interactions. For simplicity, our attention will be henceforth paid to the special case of the spin-1/2 Ising-Heisenberg tube with the isotropic Heisenberg intra-rung interaction $J_x = J_z = J$, the magnetic properties of which will be later confronted with the precise numerical results for the analogous but purely quantum spin-1/2 Heisenberg tube.

4.1. Ground-state phase diagrams

All possible ground states of the spin-1/2 Ising-Heisenberg tube can be straightforwardly obtained from the diagonalized form of the Hamiltonian (4) after taking into consideration all available combinations of quantum spin numbers involved therein. By inspection, one finds six different ground states: the classical antiferromagnetic phase (CAF)

$$|\mathrm{CAF}\rangle = \left\{ \begin{array}{l} \prod_{j=1}^{N/2} |\uparrow\uparrow\uparrow\rangle_{2j-1} \otimes |\downarrow\downarrow\downarrow\rangle_{2j} \\ \prod_{j=1}^{N/2} |\downarrow\downarrow\downarrow\rangle_{2j-1} \otimes |\uparrow\uparrow\uparrow\rangle_{2j} \end{array} \right. , \qquad (15)$$

the classical ferromagnetic phase (CFO)

$$|\mathrm{CFO}\rangle = \prod_{i=1}^{N} |\uparrow\uparrow\uparrow\rangle_i, \qquad (16)$$

the quantum antiferromagnetic phase (QAF)

$$|\mathrm{QAF}\rangle = \left\{ \begin{array}{l} \prod_{j=1}^{N/2} \left|\frac{1}{2}, L \text{ or } R\right\rangle_{2j-1} \otimes \left|-\frac{1}{2}, L \text{ or } R\right\rangle_{2j} \\ \prod_{j=1}^{N/2} \left|-\frac{1}{2}, L \text{ or } R\right\rangle_{2j-1} \otimes \left|\frac{1}{2}, L \text{ or } R\right\rangle_{2j} \end{array} \right. , \qquad (17)$$

the quantum ferromagnetic phase (QFO)

$$|\mathrm{QFO}\rangle = \prod_{j=1}^{N} \left|\frac{1}{2}, L \text{ or } R\right\rangle_j , \qquad (18)$$

the mixed classical-quantum ferrimagnetic phase (MFI)

$$|\mathrm{MFI}\rangle = \left\{ \begin{array}{l} \prod_{j=1}^{N/2} |\uparrow\uparrow\uparrow\rangle_{2j-1} \otimes \left|-\frac{1}{2}, L \text{ or } R\right\rangle_{2j} \\ \prod_{j=1}^{N/2} \left|-\frac{1}{2}, L \text{ or } R\right\rangle_{2j-1} \otimes |\uparrow\uparrow\uparrow\rangle_{2j} \end{array} \right. , \qquad (19)$$

and the mixed classical-quantum ferromagnetic phase (MFO)

$$|\mathrm{MFO}\rangle = \left\{ \begin{array}{l} \prod_{j=1}^{N/2} |\uparrow\uparrow\uparrow\rangle_{2j-1} \otimes \left|\frac{1}{2}, L \text{ or } R\right\rangle_{2j} \\ \prod_{j=1}^{N/2} \left|\frac{1}{2}, L \text{ or } R\right\rangle_{2j-1} \otimes |\uparrow\uparrow\uparrow\rangle_{2j} \end{array} \right. . \qquad (20)$$

In above, we have used the following notation for the eigenvectors of the j-th Heisenberg spin triangle $|\pm 1/2, R\rangle_j$ and $|\pm 1/2, L\rangle_j$ with the total spin $T_j^z = \pm 1/2$ and two opposite (right- and left-hand) chiralities

$$\begin{aligned} \left|\frac{1}{2}, R\right\rangle_j &= \frac{1}{\sqrt{3}} \left(|\downarrow\uparrow\uparrow\rangle + e^{\frac{2i\pi}{3}} |\uparrow\downarrow\uparrow\rangle + e^{\frac{4i\pi}{3}} |\uparrow\uparrow\downarrow\rangle \right)_j \\ \left|\frac{1}{2}, L\right\rangle_j &= \frac{1}{\sqrt{3}} \left(|\downarrow\uparrow\uparrow\rangle + e^{\frac{4i\pi}{3}} |\uparrow\downarrow\uparrow\rangle + e^{\frac{2i\pi}{3}} |\uparrow\uparrow\downarrow\rangle \right)_j \\ \left|-\frac{1}{2}, R\right\rangle_j &= \frac{1}{\sqrt{3}} \left(|\uparrow\downarrow\downarrow\rangle + e^{\frac{2i\pi}{3}} |\downarrow\uparrow\downarrow\rangle + e^{\frac{4i\pi}{3}} |\downarrow\downarrow\uparrow\rangle \right)_j \\ \left|-\frac{1}{2}, L\right\rangle_j &= \frac{1}{\sqrt{3}} \left(|\uparrow\downarrow\downarrow\rangle + e^{\frac{4i\pi}{3}} |\downarrow\uparrow\downarrow\rangle + e^{\frac{2i\pi}{3}} |\downarrow\downarrow\uparrow\rangle \right)_j \end{aligned} \qquad (21)$$

The corresponding eigenenergies per elementary triangular unit (Heisenberg spin triangle) are given by

$$\begin{aligned} E_{\mathrm{CAF}} &= -\frac{9J_1}{4} + \frac{3J}{4}, \\ E_{\mathrm{CFO}} &= \frac{9J_1}{4} + \frac{3J}{4} - \frac{3h}{2}, \\ E_{\mathrm{QAF}} &= -\frac{J_1}{4} - \frac{3J}{4}, \\ E_{\mathrm{QFO}} &= \frac{J_1}{4} - \frac{3J}{4} - \frac{h}{2}, \\ E_{\mathrm{MFI}} &= -\frac{3J_1}{4} - \frac{h}{2}, \\ E_{\mathrm{MFO}} &= \frac{3J_1}{4} - h. \end{aligned} \qquad (22)$$

It is quite obvious from the eigenvectors (15)-(20) that the four ground states CAF, QAF, MFI and MFO have a translationally-broken symmetry due to the antiferromagnetic coupling between spins from neighboring triangular units in contrast to the other two ground states CFO and QFO, which are translationally invariant. In addition, the chiral degrees of freedom of the Heisenberg spin triangles

within the eigenstates (21) with the total spin $T_j = 1/2$ are responsible for a macroscopic degeneracy of the ground states QAF, QFO, MFI and MFO. The ground state QAF has the largest residual entropy $S = (N+1)k_B \ln 2$ due to a mutual interplay of translationally broken symmetry and chiral degrees of freedom, the ground state QFO has the residual entropy $S = Nk_B \ln 2$ originating solely from the chiral degrees of freedom, while the latter two ground states MFI and MFO have the residual entropy $S = (N/2+1)k_B \ln 2$ coming from the translationally broken symmetry and chiral degrees of freedom.

The ground-state phase diagram of the spin-1/2 Ising-Heisenberg triangular tube is depicted in Fig. 2(a). At zero magnetic field $h = 0$ the antiferromagnetic phases QAF and CAF with a zero net magnetization emerge as the only two possible ground states. The ground state QAF of a quantum character is stable in a parameter region with the predominant Heisenberg intra-rung interaction $J_1/J < 3/4$, while the ground state CAF of a classical nature is stable in a parameter region with the predominant Ising inter-rung interaction $J_1/J > 3/4$. Of course, the antiferromagnetic order inherent to the ground states QAF or CAF breaks down when the external magnetic field approaches its first critical value h_{c1}, above which another two unusual quantum ground states QFO and MFI appear. It is evident from Fig. 2(a) that the ground state QAF turns to the QFO phase at the critical field $h_{c1} = J_1$, while the ground state CAF evolves into the MFI phase at the critical field $h_{c1} = 3J_1 - 3J/2$. The ground states QFO and MFI are stable at moderate values of the magnetic field ranging up to the second critical fields $h_{c2} = J_1 + 3J/2$ and $3J_1$, respectively, which represent a lower boundary for a presence of the ground state MFO with a modulated ferromagnetic character. Finally, all spins are forced to align within the fully polarized ground state CF for the stronger magnetic fields than the saturation field $h_{c3} = 3J_1 + 3J/2$.

To compare with, the ground-state phase diagram of the fully quantum spin-1/2 Heisenberg triangular tube is shown in Fig. 2(b). Both ground-state phase diagrams generally display several common features especially for small enough values of the interaction ratio $J_1/J < 1/2$, while they show quite distinct features mainly for larger values of the interaction ratio $J_1/J > 1/2$. At low enough magnetic fields, the ground state of the spin-1/2 Heisenberg tube can be effectively described either by the spin-liquid state of the spin-1/2 Heisenberg chain (for $J_1/J < 0.629$), or by the spin-liquid state of the spin-3/2 Heisenberg chain (for $J_1/J > 0.629$). In any case, both phases are gapless and can be characterized by a continuous change of the magnetization upon rising the magnetic field. This finding represents quite distinct feature of the spin-1/2 Heisenberg tube, which cannot be in principle found in the analogous spin-1/2 Ising-Heisenberg tube regardless of a relative strength of both considered coupling constants.

However, the energy gap of the effective spin-1/2 Heisenberg chain closes at the critical field $h_{c1} = 2J_1$, whereas the fully polarized state of this effective model is the lowest-energy state of the spin-1/2 Heisenberg tube unless the second critical field $h_{c2} = J_1 + 3J/2$ is reached. It is quite apparent that the fully polarized state of the effective spin-1/2 Heisenberg chain, as the ground state of the spin-1/2 Heisenberg tube, exactly coincides with the ground state QFO of the spin-1/2 Ising-Heisenberg tube given by the eigenvector (18). Similarly, the fully polarized state of the effective mixed spin-(1/2,3/2) Heisenberg chain, which appears as another ground state of the spin-1/2 Heisenberg tube in between the second and third critical fields $h_{c2} = J_1 + 3J/2$ and $h_{c3} = 3J_1 + 3J/2$, can be exactly identified with the ground state MFO of the spin-1/2 Ising-Heisenberg tube given by the eigenvector (20). As a matter of fact, this eigenstate is delimited precisely by the same critical fields as reported for the ground state MFO of the spin-1/2 Ising-Heisenberg tube. It can be thus concluded that there is a perfect coincidence between the ground-state phase diagrams of the spin-1/2 Ising-Heisenberg and Heisenberg tube in a parameter space $J_1/J < 1/2$ and $h > 2J_1$, i.e. once the interaction ratio J_1/J is sufficiently small and the energy gap of the effective spin-1/2 Heisenberg chain is closed by the magnetic field.

Contrary to this, the ground-state phase diagrams of the spin-1/2 Ising-Heisenberg and Heisenberg tube differ basically at moderate and sufficiently strong values of the interaction ratio $J_1/J > 1/2$ [c.f. Fig. 2(a) with Fig. 2(c)]. In addition to three gapless ground states of the spin-1/2 Heisenberg tube, which correspond to the effective spin-1/2, mixed spin-(1/2,3/2) and spin-3/2 Heisenberg chains, one novel gapful phase inherent to the intermediate one-half plateau of the effective mixed spin-(1/2,3/2) Heisenberg chain can be found at moderate values of h/J and

J_1/J. The intermediate one-half plateau of the effective mixed spin-(1/2,3/2) Heisenberg chain gives rise to the novel one-third plateau of the spin-1/2 Heisenberg tube, which is of completely different origin than the one-third plateau originating from the fully polarized state of the effective spin-1/2 Heisenberg chain. It should be pointed out, moreover, that the ground state MFI of the spin-1/2 Ising-Heisenberg tube cannot capture spin arrangements of none of these novel quantum ground states of the spin-1/2 Heisenberg tube.

4.2. Magnetization process

Next, let us examine zero-temperature magnetization curves of the spin-1/2 Ising-Heisenberg and Heisenberg triangular tubes. According to the Oshikawa-Yamanaka-Affleck rule, the spin-1/2 triangular tube may possibly exhibit intermediate magnetization plateaus at zero, one-third and two-thirds of the saturation magnetization when the doubling of unit cell is taken into consideration. It can be seen from Fig. 3(a) that the spin-1/2 Ising-Heisenberg tube exhibits all available magnetization plateaus. More specifically, the antiferromagnetic ground states QAF and CAF are responsible for a trivial plateau with zero net magnetization, the ground states QFO and MFI are pertinent to the intermediate one-third magnetization plateau and finally, the ground state MFO is respective realization of the two-thirds magnetization plateau. Hence, it follows that the zero, one-third and two-thirds magnetization plateaus are always present in the zero-temperature magnetization curve of the spin-1/2 Ising-Heisenberg tube even though the underlying mechanism for the plateau formation depends basically on whether the interaction ratio is greater or smaller than the speficic value $J_1/J = 3/4$. In the former case $J_1/J < 3/4$ the zero and one-third magnetization plateaus correspond to the ground states QAF and QFO, while the zero and one-third magnetization plateaus appear as a result of the ground states CAF and MFI in the latter case with $J_1/J > 3/4$.

The zero-temperature magnetization process of the spin-1/2 Heisenberg triangular tube can be obtained from DMRG data for the lowest-energy states of the three effective spin-chain models (12)-(14) calculated separately for each sector with the total spin S^z_T. The magnetic field, at which the magnetization undergoes the respective change of the total spin from S^z_T to $S^z_T + 1$, can be calculated from the difference between the lowest-energy levels from adjacent sectors $h = E_g^{h=0}(N, S^z_T + 1) - E_g^{h=0}(N, S^z_T)$ at zero magnetic field. Fig. 3(b) illustrates a 3D plot of the magnetization against the relative strength of the interaction ratio J_1/J and the magnetic field h/J. As one can see, the magnetization continuously varies from zero up to the saturation value upon strengthening of the magnetic field on assumption that the interaction ratio J_1/J is sufficiently large. Under this condition, the spin-1/2 Heisenberg tube does not display any intermediate magnetization plateau. Contrary to this, the magnetization shows a smooth change with the rising magnetic field only until the one-third magnetization plateau is reached when the interaction ratio is sufficiently small $J_1/J < 1/2$. The one-third plateau is subsequently followed by an abrupt magnetization jump towards a narrower two-thirds plateau, which ends up at the saturation field where the magnetization jumps to its saturation value. It should be nevertheless mentioned that the most striking magnetization curves can be detected at moderate values of the interaction ratio $0.5 < J_1/J \lesssim 0.64$, which may involve a continuous change of the magnetization in between the intermediate plateaus due to the presence of the gapless spin-liquid ground states.

4.3. Bipartite entanglement

It is quite evident from the Ising character of the inter-rung interaction assumed within the spin-1/2 Ising-Heisenberg triangular tube that there is no correlation between transverse components of two spins from neighboring triangular cells. As a result, the spin-1/2 Ising-Heisenberg tube does not exhibit quantum correlations between spins from distinct triangular units in contrast to the spins belonging to the same triangular unit, which may display a quantum entanglement due to a quantum character of the Heisenberg intra-rung coupling. With this background, we have computed for all available ground states the longitudinal and transverse components of the correlation function between two spins from the same triangular unit along with the local magnetization in order to determine from Eq. (9) the concurrence as a quantum entanglement estimator. The resulting diagram for the concurrence is plotted in Fig. 4. As it could be expected, there is no quantum entanglement in the classical ground states CF and CAF, while the other four ground

states QAF, QFO, MFI and MFO display quantum correlations evidenced by non-zero concurrence. Two spatial components of the pair correlation function and local magnetization for any two spins from the same triangular unit equal within the ground states QAF and QFO to $C_{xx} = C_{zz} = -1/12$ and $m = \pm 1/6$, which implies the following value $C = 1/3$ of the concurrence. Though any two spins from the same triangular cell are quantum-mechanically entangled, the bipartite entanglement is incomplete due to the Heisenberg intra-rung coupling with the third spin. Quantum entanglement and frustration on clusters with integer spins has been recently investigated showing also distinct trends in the various ordered phases[29].

The more subtle situation can be observed within the mixed classical-quantum ground states MFI and MFO, where the bipartite entanglement between two spins from the same triangular unit basically depends on a regular alternation of the classical state $|\uparrow\uparrow\uparrow\rangle$ with the quantum state $|\pm 1/2, \mathrm{L\ or\ R}\rangle$, see the eigenvectors (19) and (20). Of course, the former classical state $|\uparrow\uparrow\uparrow\rangle$ is consistent with the absence of quantum correlations C=0 in accordance with $C_{xx} = 0$, $C_{zz} = 1/4$ and $m = 1/2$, while the latter quantum state $|\pm 1/2, \mathrm{L\ or\ R}\rangle$ indicates the same incomplete bipartite entanglement C=1/3 as reported for the ground states QAF and QFO with regard to $C_{xx} = C_{zz} = -1/12$ and $m = \pm 1/6$. Thus, one may conjecture for the modulated classical-quantum ground states MFI and MFO the mean value of the concurrence $C = 1/6$, which measures the bipartite entanglement between two spins from the same triangular unit.

The most profound difference between the spin-1/2 Ising-Heisenberg and Heisenberg tube is that the former spin model shows absence of quantum correlations between the spins from distinct triangular unit cells in contrast with the latter fully quantum spin model. To clarify this issue in a more detail, we have calculated for the spin-1/2 Heisenberg tube using the DMRG method two spatial components of the pair correlation function between the spins from neighboring triangular units. The corresponding results for the correlation functions $C_{xx} = \langle \hat{S}^x_{i,j} \hat{S}^x_{i+1,j} \rangle$ and $C_{zz} = \langle \hat{S}^z_{i,j} \hat{S}^z_{i+1,j} \rangle$ are plotted in Fig. 5 against the interaction ratio J_1/J and the magnetic field h/J. As could be expected, the correlation functions C_{xx} and C_{zz} exhibit plateaus in the parameter region corresponding to the gapful ground states, while they show a continuous variation within the parameter space corresponding to the gapless ground states. Apparently, the transverse correlation C_{xx} between the spins from neighboring triangular units equals zero in all gapful ground states, which excludes a possible occurrence of the respective bipartite entanglement.

The quantum entanglement between the spins from neighboring unit cells can be accordingly found just within the gapless ground states. Fig. 6 illustrates typical dependences of the concurrence on the interaction ratio J_1/J and the magnetic field h/J, which serve in evidence of the quantum entanglement in the gapless ground state described by the effective spin-3/2 Heisenberg chain. It is quite evident from Fig. 6 that the concurrence monotonically decreases with the magnetic field due to a gradual degradation of quantum fluctuations and reinforcement of the spin polarization. It should be pointed out, however, that the concurrence vanishes well before the magnetization reaches the full polarization. Another interesting observation is that the spins from neighboring triangular units are not quantum-mechanically entangled within the other gapless ground state, which correspond to the effective spin-1/2 Heisenberg chain. This finding is rather surprising with respect to stronger quantum fluctuations of the effective spin-1/2 Heisenberg chain, which substantially suppress the relative strength of both spatial components C_{xx} and C_{zz} of the pair correlation function between the spins from neighboring triangular units (see Fig. 5).

5. Conclusion

In summary, we have provided a detailed comparison of the ground-state properties of the frustrated spin-1/2 Ising-Heisenberg and Heisenberg triangular tubes in a presence of the external magnetic field, which differ from each other by character of the inter-rung interaction (Ising vs. Heisenberg). All available ground states of the spin-1/2 Ising-Heisenberg triangular tube were rigorously found and the overall ground-state phase diagram constructed. The ground-state phase diagram of the spin-1/2 Ising-Heisenberg tube involves the four quantum ground states QAF, QFO, MFI and MFO in addition to two classical ground states CAF and CF. Each couple of the spins from one and the same triangular unit is quantum-mechanically entangled within the ground states

QAF and QFO, while the quantum entanglement between the nearest-neighbor spins is only present in each second triangular unit within the mixed classical-quantum ground states MFI and MFO. The quantum entanglement between the nearest-neighbor spins from the same triangular unit cell was confirmed through the non-zero value of the concurrence serving as a measure of bipartite entanglement.

To compare with, the ground-state phase diagram of the spin-1/2 Heisenberg triangular tube constructed on the grounds of DMRG calculations [17] includes in total one classical ground state, three gapped quantum ground states and three gapless quantum ground states. The classical ground state and two gapped quantum ground states can be exactly identified with the three ground states CF, QFO and MFO of the spin-1/2 Ising-Heisenberg tube. Owing to this fact, there is a perfect coincidence between the ground-state phase diagrams of the spin-1/2 Ising-Heisenberg and Heisenberg tube in a parameter region $J_1/J < 1/2$ and $h > 2J_1$ inherent to those ground states. In the rest of the parameter space, there appear substantial differences connected mainly with a presence of gapless quantum ground states with a spin-liquid character. Consequently, the magnetization scenario of the spin-1/2 Heisenberg tube is much more miscellaneous in comparison with the magnetization process of the spin-1/2 Ising-Heisenberg tube, which always involves the zero, one-third and two-thirds plateaus and respective magnetization jumps in between them. The magnetization curve of the spin-1/2 Heisenberg tube never contains just the plateau at zero magnetization, but it may contain or not the intermediate one-third and two-thirds plateaus of different origin depending on the relative strength of the inter-rung and intra-rung coupling constants. In addition, the spin-1/2 Heisenberg tube may exhibit bipartite entanglement evidenced by non-zero concurrence between spins from distinct triangular unit cells within the gapless spin-liquid ground state.

Acknowledgments

This work was partially supported by CNPq, CAPES, and FINEP (Federal Brazilian Agencies), CNPq-Rede Nanobioestruturas, as well as FAPEAL (Alagoas State Agency). R.C.A. thanks CAPES for financial support, and Faculty of Science of P. J. Šafárik University in Košice - Slovakia for the afforded hospitality. J.S. acknowledges financial support of Ministry of Education of Slovak Republic provided under the VEGA grant No. 1/0043/16 and by the grant of the Slovak Research and Development Agency under the contract Nos. APVV-0097-12 and APVV-14-0073.

[1] *Introduction to Frustrated Magnetism*, eds.: C. Lacroix, Ph. Mendels, F. Mila, Springer, Heidelberg, 2011.

[2] L. Amico, R. Fazio, A. Osterloh, V. Vedral, Rev. Mod. Phys. **80**, 517 (2008).

[3] R. Horodecki, P. Horodecki, M. Horodecki, K. Horodecki, Rev. Mod. Phys. **82**, 865 (2009).

[4] G. Toulouse, Commun. Phys. **2**, 115 (1977).

[5] *Frustrated Spin Systems*, ed.: H. T. Diep, World Scientific, Singapore, 2004.

[6] M.P. Gelfand, Phys. Rev. B **43**, 8644 (1991).

[7] Y. Xian, J. Phys.: Condens. Matter **6**, 5965 (1994).

[8] Y. Xian, Phys. Rev. B **52**, 12485 (1995).

[9] E.H. Kim, O. Legeza, J. Solyom, Phys. Rev. B **77**, 205121 (2008).

[10] M. Sato, Phys. Rev. B **72**, 104438 (2005).

[11] B. Sutherland, Phys. Rev. B **62**, 11499 (2000).

[12] R. Citro, E. Orignac, N. Andrei, C. Itoi, S. Qin, J. Phys.: Condens. Matter **12**, 3041 (2000).

[13] R.-X. Li, S.-L. Wang, Y. Ni, K.-L. Yao, H.-H. Fu, Phys. Lett. A **378**, 970 (2014).

[14] M. Takigawa, F. Mila, in *Introduction to Frustrated Magnetism*, eds.: C. Lacroix, Ph. Mendels, F. Mila, Springer, Heidelberg, 2011, pp.241–269.

[15] M. Oshikawa, M. Yamanaka, I. Affleck, Phys. Rev. Lett. **78**, 1984 (1997).

[16] I. Affleck, Phys. Rev. B **37**, 5186 (1998).

[17] A. Honecker, F. Mila, M. Troyer, Eur. Phys. J. B **15**, 227 (2000).

[18] J. Schnack, H. Nojiri, P. Kögerler, G.J.T. Cooper, L. Cronin, Phys. Rev. B **70**, 174420 (2004).

[19] N.B. Ivanov, J. Schnack, R. Schnalle, J. Richter, P. Kögerler, G.N. Newton, G.J.T. Cooper, L. Cronin, Y. Oshima, H. Nojiri, Phys. Rev. Lett. **105**, 037206 (2010).

[20] M. Sato, Phys. Rev. B **75**, 174407 (2007).

[21] M. Sato, T.Sakai, Phys. Rev. B **75**, 014411 (2007).

[22] T. Sakai, M. Sato, K. Okunishi, Y. Otsuka, K. Okamoto, C. Itoi, Phys. Rev. B **78**, 184415 (2008).

[23] J. Strečka, R.C. Alécio, M.L. Lyra, O. Rojas, J. Magn. Magn. Mater. **409**, 124 (2016).

[24] W. K. Wootters, Phys. Rev. Lett. **80**, 2245 (1998).

[25] L. Amico, A. Osterloh, F. Plastina, and R. Fazio, Phys. Rev. A **69**, 022304 (2004).

[26] H. L. Huang, B. Wang, Z. Y. Sun, and S. P. Kou, Chin. Phys. Lett. **185**, 30 (2014).

[27] S. R. White, Phys. Rev. Lett. **69**, 19 (1992).

[28] B. Bauer *et al*, J. Stat. Mech. P05001 (2011).

[29] V. S. Abgaryan, N. S. Ananikian, L. N. Ananikyan, and A. N. Kocharian, Phys. Scr. **83**, 055702 (2011).

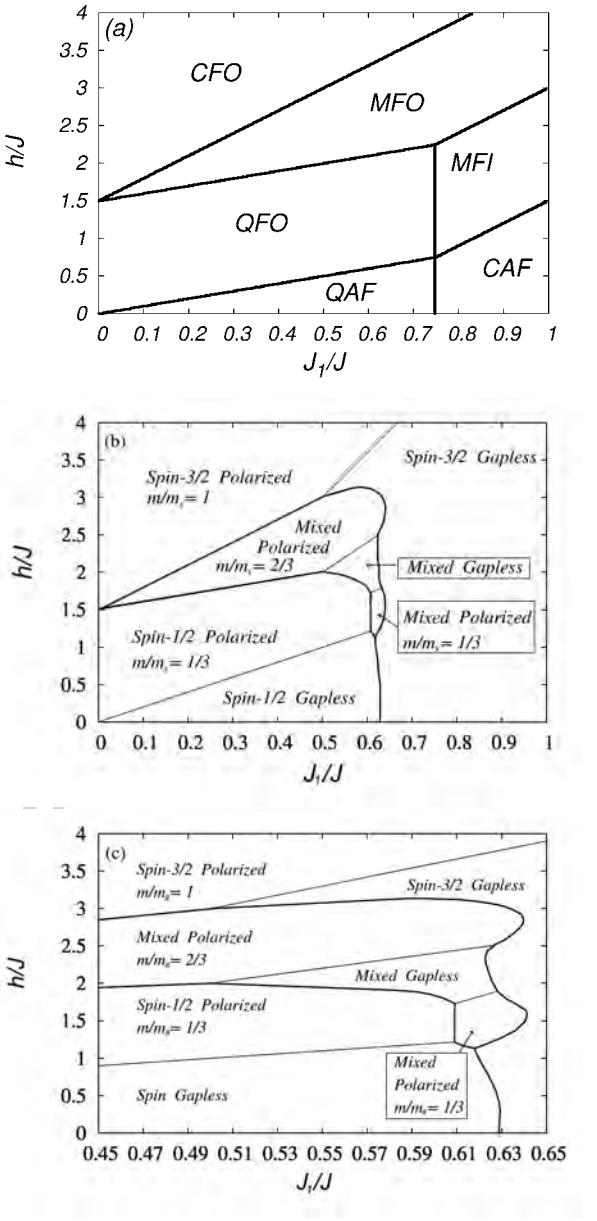

Figure 2: (a) Ground-state phase diagram of the spin-1/2 Ising-Heisenberg tube in $J_1/J - h/J$ plane, which consists of six distinct gapped phases. (b) Ground-state phase diagram of the spin-1/2 Heisenberg tube in $J_1/J - h/J$ plane, which constitute four gapped and three gapless phases. (c) A detail from the ground-state phase diagram of the spin-1/2 Heisenberg tube, which shows a reentrant character of the phase boundary related to the effective spin-3/2 gapless phase. Thick (thin) lines denote first-order (second-order) phase transitions.

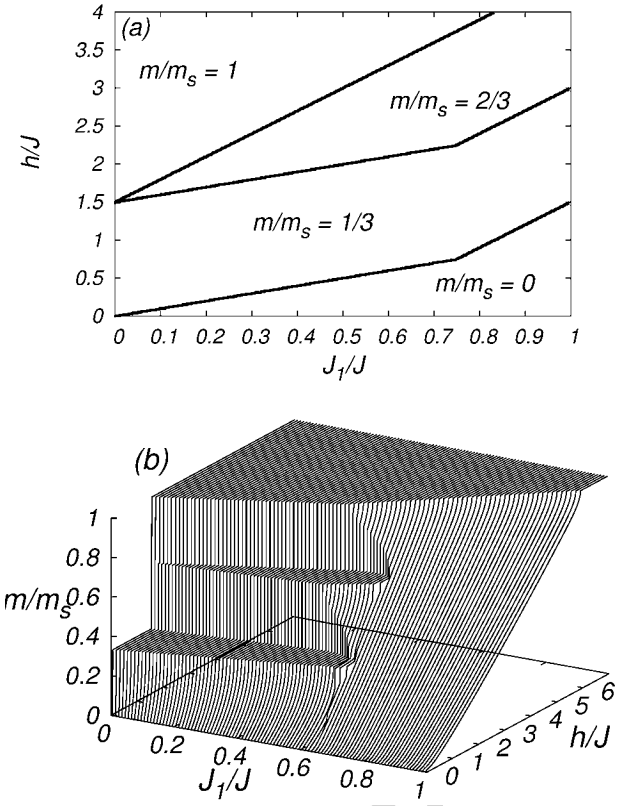

Figure 3: The magnetization normalized with respect to the saturation value as a function the interaction ratio J_1/J and the magnetic field h/J for: (a) the spin-1/2 Ising-Heisenberg tube; (b) the spin-1/2 Heisenberg tube.

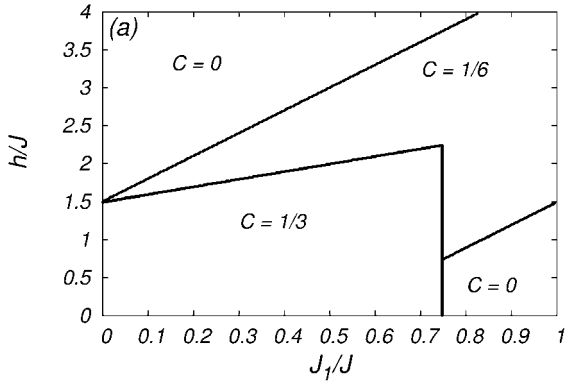

Figure 4: The concurrence for two spins coupled within the spin-1/2 Ising-Heisenberg tube through the Heisenberg intra-triangle interaction as a function of the interaction ratio J_1/J and the magnetic field h/J.

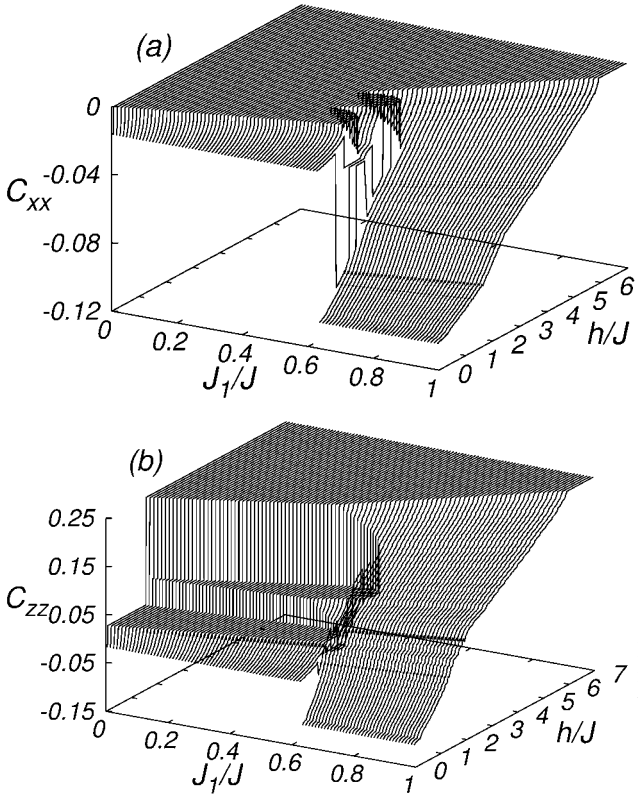

Figure 5: Both spatial components of the inter-rung pair correlation function C_{xx} and C_{zz} as a function of the interaction ratio J_1/J and the magnetic field h/J within the spin-1/2 Heisenberg tube.

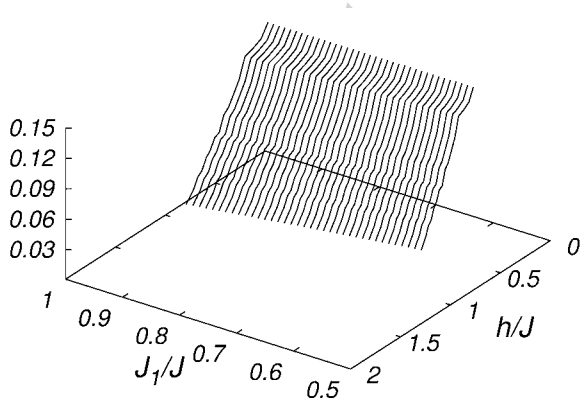

Figure 6: The concurrence between two spins from neighboring triangular units of the spin-1/2 Heisenberg tube as a function of the interaction ratio J_1/J and the magnetic field h/J. The incomplete entanglement, which occurs just within the gapless ground state corresponding to the effective spin-3/2 Heisenberg chain, is gradually suppressed as the magnetic field strengthens.